Volume 17, Number 2, 2024. pp. 207-216

Jordan Journal of Physics

ARTICLE

Fabrication and Characterization of Field Emission Electron Source Based on Deploying Multiwall Carbon Nanotubes in Micro Dine Point Capillary Tubes

Marwan S. Mousa[a], **Batool M. Almarzok**[a] and **Mark J. Hagmann**[b]

[a] *Surface Physics and Materials Technology Lab, Department of Physics, Mu'tah University, Al-Karak, 61710, Jordan.*

[b] *Department of Electrical and Computer Engineering, University of Utah, 50 S. Central Campus Dr #2110, Salt Lake City, Utah 84112, USA.*

Doi: **https://doi.org/10.47011/17.2.8**

Received on: 15/02/2023; *Accepted on: 06/11/2023*

Abstract: Thin multiwall carbon nanotubes (MWCNTs), produced by chemical vapor deposition, were employed in this study. These MWCNTs were inserted into capillary tubes, which were heated and pulled to form fine points, compressing the exposed ends of the nanotubes to create field emitters. This technique does not require the addition of pitch, epoxy resins, or any other types of coating or binding materials typically used to increase electrical and thermal resistance. In addition, the study reports the measured current-voltage characteristics of these emitters, the corresponding Fowler-Nordheim plots, the field emission microscope patterns, and the scanning electron micrographs for the prepared samples.

Keywords: Multiwall carbon nanotubes, Pyrex capillary tubes, Electron source, Fowler-nordheim plots, Field electron emission.

Introduction

Carbon nanotubes (CNTs) were discovered by Iijima in 1991 [1] and were later synthesized by others [2-4]. They consist of graphene monolayers rolled into cylindrical sheets with diameters ranging from 1 to 50 nm [5]. The promising applications of CNTs range from nanotube composite materials to nanoelectronics [6, 7]. Multiwall carbon nanotubes (MWCNTs) have remarkable properties as field emitters, such as a high aspect ratio (>150), a small radius of beam curvature, high chemical stability, and high mechanical strength [5, 8, 9].

Previous studies have reported using MACNTs as a field electron emission source when mounted in the glass. The reports focused on understanding the high-voltage breakdown [10-12], creating stable bright electron sources, and developing the field emission theory from metal-insulator composites and glass [13-15].

The first demonstration of the field emission capabilities of MWCNTs was conducted in 1995 by Heer *et al.* The experimental setup included a small electron gun with a 1 mm diameter MWCNTs film serving as the cathode, and an extraction grid positioned 20 μm away from the same film acting as the anode. They achieved a current density of 100 $\mu A/cm^2$ at an operating voltage of 200 V. In this research, the obtained results were validated by the Fowler-Nordheim theory and analysis of field electron emission [16].

The results from the Heer group sparked a huge research interest in field emissions from

Corresponding Author: Marwan S. Mousa **Email**: mmousa@mutah.edu.jo

CNTs, a trend that has continued to increase over time. Moreover, literature has previously reported field electron emission from CNTs mounted in glass with a conductive coating [17-19].

Field electron emission is the process of emitting electrons from the surface of a metallic cathode under the influence of an intense applied electric field (> 3×10^9 V/m) [20, 21], where the emission current depends strongly on the work function of the emitter. This paper introduces a new type of emitter based on MWCNTs and presents the fabrication techniques along with field emission data.

Materials and Methods

We used NanocylTM NC 7000 MWCNTs prepared by catalytic chemical vapor deposition (CCVD) at Nanocyl S. A. (Sambre Ville, Belgium). In CCVD, solid carbon is precipitated by chemical and thermal processes in the presence of a metal catalyst [22]. A pulling process at high temperatures prepared fine glass capillary tubes, and the tips at the smaller end were cut. Then the MWCNTs were inserted into each tube to protrude from the tip end [23].

Fig. 1(a) shows the glass-pulling device in which a frame has bearings positioned accurately on plates supported by three stainless steel rods attached to the frame of the puller control unit, serving as a base for the instrument. Each glass tube, with an outer diameter of 1 mm and an inner diameter of 0.1 mm, fits inside these bearings between the upper and lower chuck spindles, with a heating coil located around it, as shown in Fig. 1(b). The temperature of the heating coil can be increased to 1400 K, which is the softening point of the borosilicate glass the tubes are made of. When the tube starts to melt, the weight of the chuck spindle causes it to slide down vertically, pulling the glass tube and turning off the circuit, creating boracic micro-glass tips [17-19]. Nanocyl^{TM} NC 7000 MWCNTs, with a diameter of 9.5 nm and an aspect ratio higher than 150%, were used in this experiment (Nanocyl S.A., Sambreville, Belgium). After filling each tube with the MWCNTs, a tungsten wire with a diameter of 0.1 mm was used from the other tube entrance to make the electrical connection with the MWCNTs.

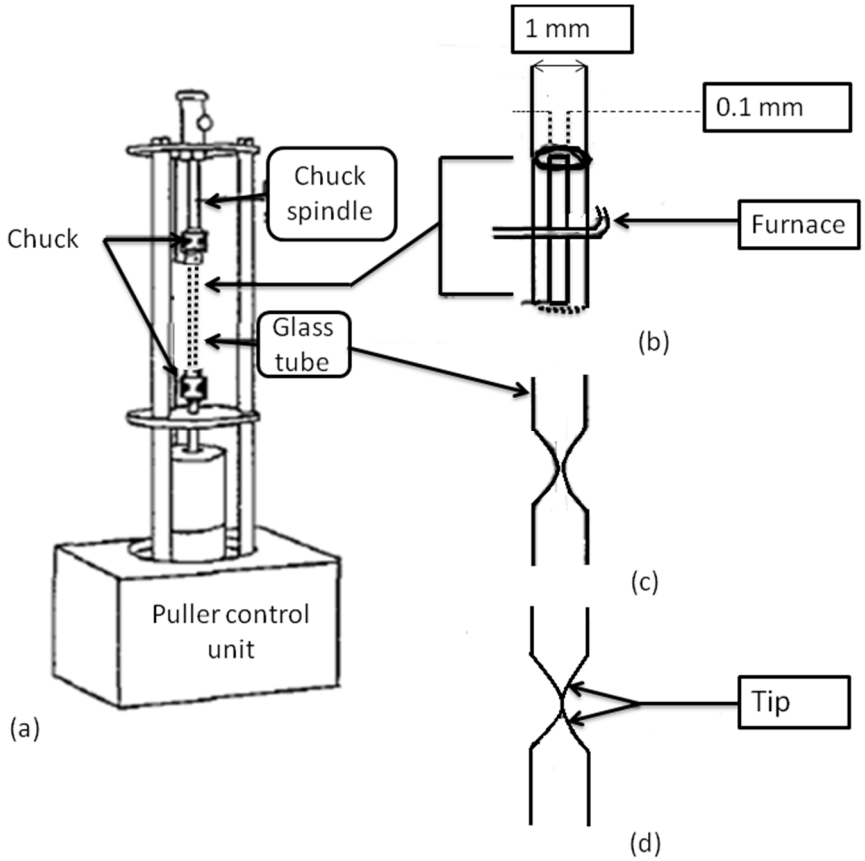

FIG. 1. (a) Glass-pulling device, (b) glass tube before pulling, (c) glass tube during pulling shows smooth needle-like emitter, (d) the glass tips were cut and filled by the MWCNTs.

The measurements and analyses of the current-voltage (I-V) and emission images were carried out in a traditional field emission microscope, where the axial electrode separation was approximately 10 mm. The typical operating pressure was ~10^{-7} mbar provided by a system of rotary pumps and a silicon oil diffusion pump. The vacuum level can be improved by decreasing the pressure to ~10^{-9} mbar after baking the system at ~200 ºC for ~12 hours. The potential applied to each emitter was slowly increased. Some emitters had a switch-on voltage (V_{SW}) similar to earlier phenomena [17]. The low field region of the current-voltage (I-V) data is consistent with the Fowler-Nordheim (FN) analysis, as will be discussed in the following section [24, 20]. The scanning electron microscope (SEM) images were provided at different magnifications to report the MWCNTs inside the used micro-glass tubes.

Results and Discussion

The total electron emission current I was plotted versus the applied voltage between the emitter and anode in several modes, including an FN plot. A digital camera recorded the field emission microscope (FEM) images formed on a screen (anode) by the electrons. The applied field was increased slowly to avoid current surges. The SEM images of two types of emitters are presented in Fig. 2.

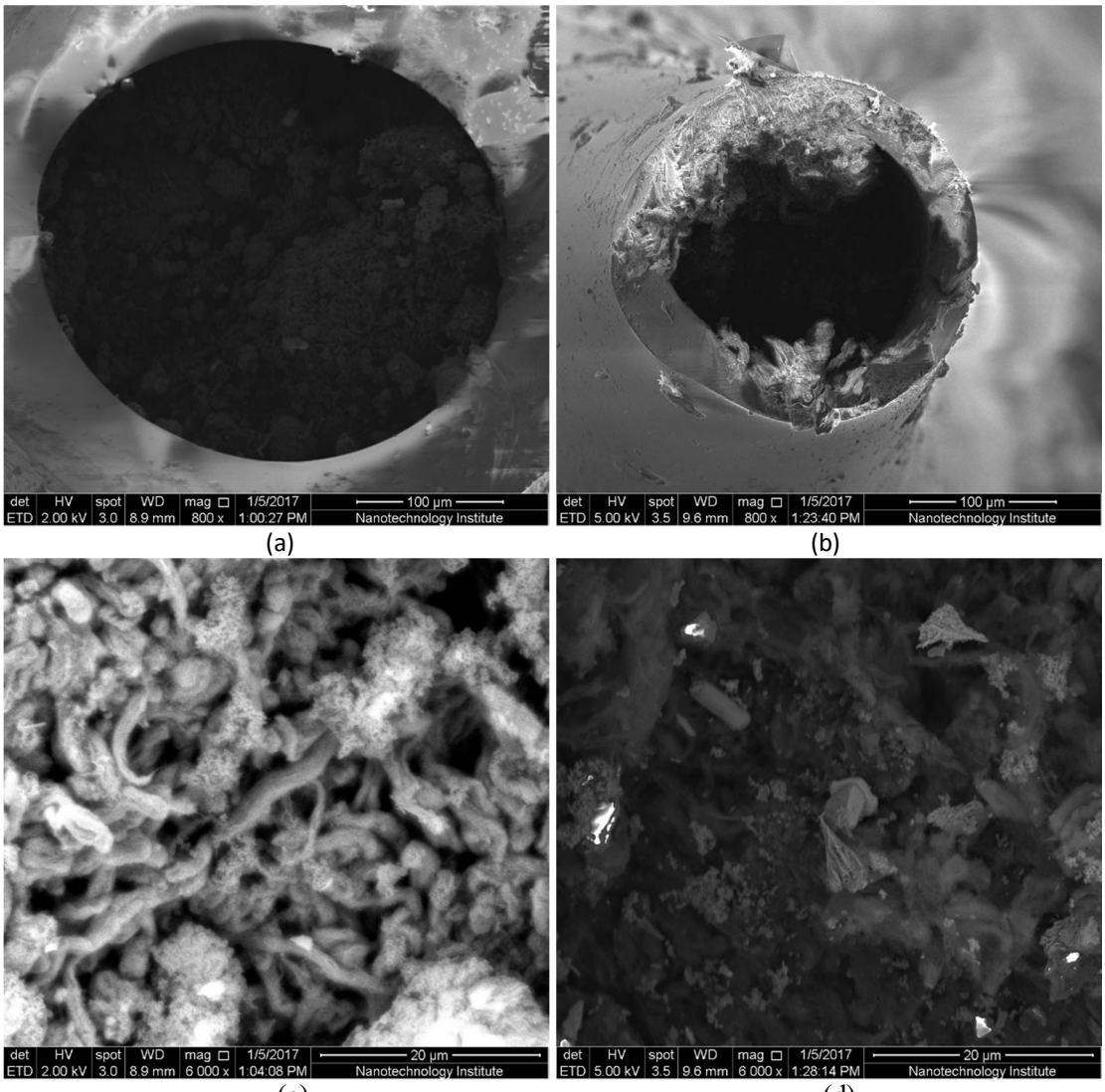

FIG. 2. Scanning electron microscope images of the fabricated field emitter for (a) emitter 1, which has a tapered end with an opening diameter of 315 µm, (b) emitter 2, which has an opening diameter of 184 µm, (c) the MWCNT surface of emitter 1, and (d) the MWCNT surface of emitter 2.

The SEM images in Figs. 2(a) and 2(b) show that the two emitters have an elliptical shape. The major axis for emitter 1, shown in Fig. 2(a), is 315 µm, whereas the major axis for emitter 2 in Fig. 2(b) is 184 µm. Powder from the MWCNTs is seen at the open end of the glass emitter nearest to the anode. After filling the glass sample with MWCNTs, an agglomerate of MWCNTs was mechanically added to the micro aperture to ensure good electric field penetration to the nanotubes. Moreover, an EDX (energy dispersive X-ray spectroscopy) analyzer was used to ensure that the aperture surface was composed of carbon.

In Fig. 3(a), for emitter 1, the applied voltage was slowly increased from 1,500 V, with a threshold current of 9.9 pA, to 6,000 V, with a current of 360 nA. Then switch-on to saturation occurred at 6,100 V for a current of 50 µA. Following the switch-on, the current decreased proportionately to the applied voltage as the potential decreased to 2,000 V for a current of 10 µA. Further voltage reduction caused the current to fall to nearly zero, reaching the threshold values V_{TH} = 1,600 V and I_{TH} = 9.7 pA.

In Fig. 3(b), the slope was –133,994 V/decade for the forward scan plot, and the slope for the reverse scan plot in the low field region was –103,095 V/decade. In Fig. 3(b), the FN plot shows a straight-line segment with a positive slope during the decreasing part of the voltage cycle. This behavior has been previously reported to be connected to the existence of a series safety resistor. The existence of the resistor causes saturation in FN plots because of the approaching maximum current in the original I-V characteristics [25]. However, the fact that the obtained I-V characteristics are close to the theoretical assumptions shows that, in some cases, the previously presented assumption about the interpretation of FN plots is incorrect. Thus, new terminology is needed to describe this behavior in FN plots. The FN-plot turnover suggests that it may or may not be associated with current saturation [26]. Among the possibilities suggested in the literature, this effect can also be subjected to the emission current dependence in the field enhancement factor [26]. The second current-voltage cycle for the emitter 1 is shown in Fig. 4.

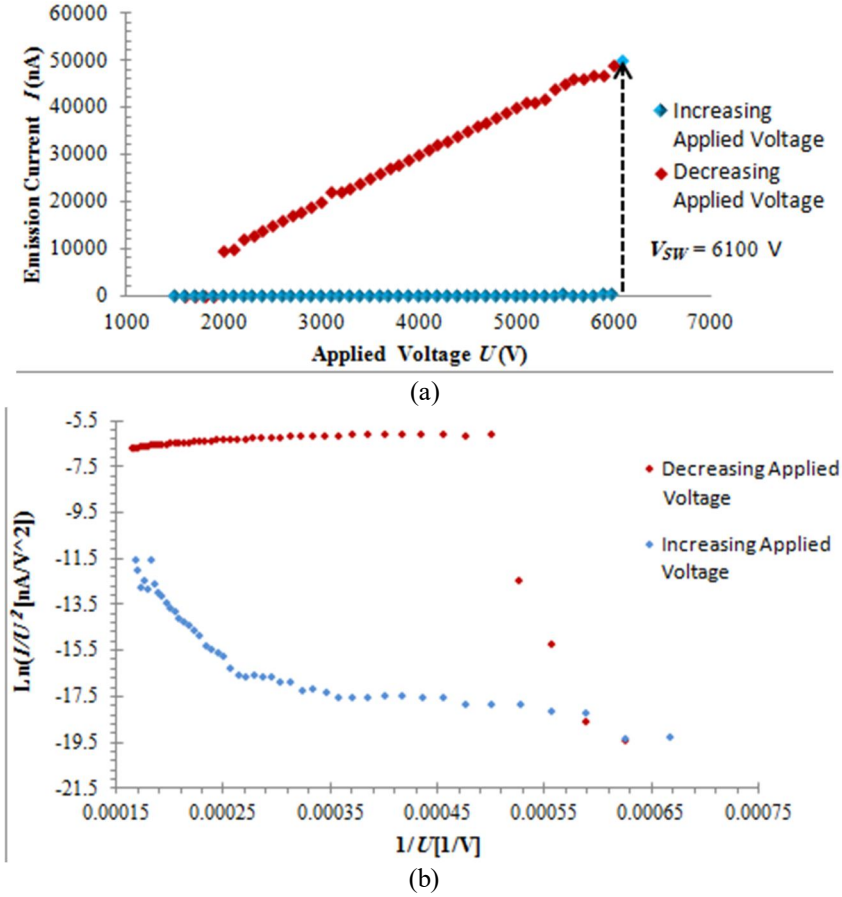

FIG. 3. First cycle of applied voltage while increasing and decreasing the voltage: (a) I-V characteristics of MWCNT emitter and (b) corresponding FN plot for the increasing and decreasing cycle.

Fig. 4(a) for emitter 1 shows that the emission current was 100 nA at an applied potential of 6,000 V. However, when the applied voltage was increased to 6,100 V, the switch-on occurred, transitioning the current to 52 µA. Fig. 4(a) shows that at the maximum applied voltage, V_{MAX} = 7,400 V, the current remained at I_{MAX} = 52 µA. Then, as the voltage was reduced, the "saturated" region extended to 6,100 V while the current remained at 52 µA. Further voltage reduction caused the emission current to fall to nearly zero, reaching the threshold values V_{TH} = 1,700 V and I_{TH} = 9.9 pA.

Fig. 4(b) shows that the Fowler-Nordheim region of current has shifted to a lower applied voltage. The shift of the emission current to lower voltages may occur either because of surface impurities or the creation of multiple emitting sites that switch on at different voltages [18, 27].

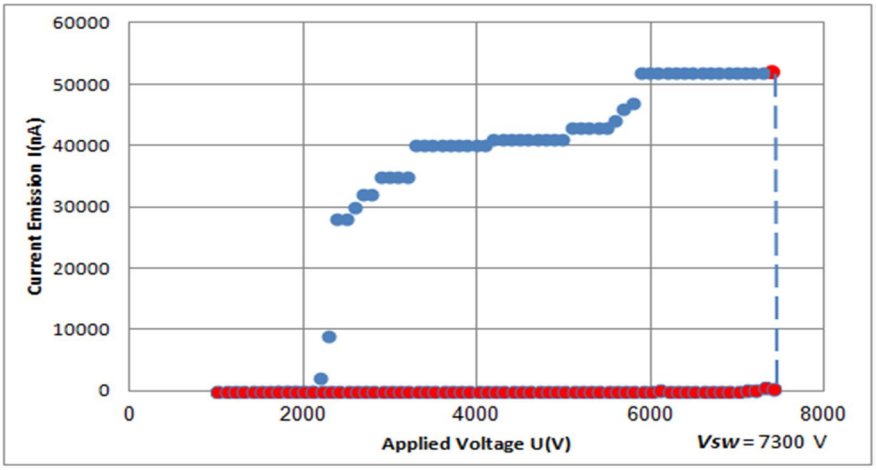

(a)

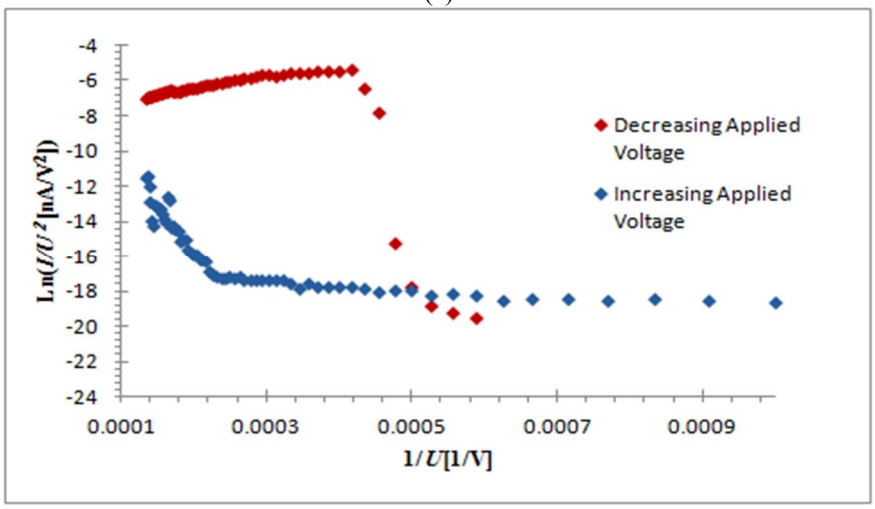

(b)

FIG. 4. Second decreasing applied voltage cycle: (a) emission current (nA) of MWCNT emitter one versus applied voltage (V) and (b) FN plot showing saturation at high emission current. The range of data gives a linear FN plot at low field region (with slope = –94,031 V/decade).

Fig. 5 shows the electron emission images captured on the tin-oxide-coated phosphor screen (anode) of the field emission microscope. Before switch-on, the image shows a concentrated spot with discernible structure, as shown in Figs. 6(a) and 6(b). At higher currents, Fig. 6(a) and 6(b) reveal a significantly larger spot with a marvelous structure.

Current-voltage measurements were also made for the smooth needle-like emitter number 2, as shown in Figs. 6(a) and 6(b). SEM images for this sample are presented in Figs. 2(b) and 2(d), with the field emission pattern concentrated as shown in Fig. 6(c). The voltage was cycled three times to obtain the concentrated emission image.

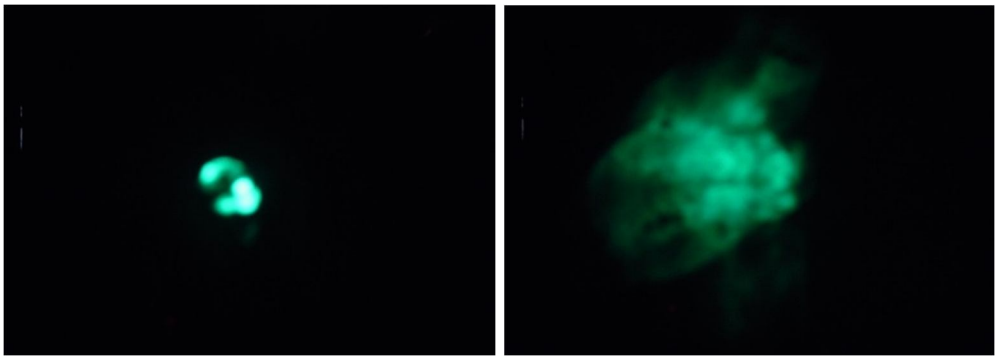

(a) (b)

FIG. 5. Emission image obtained at (a) (V = 7,100 V, I = 120 nA), (b) (*VMAX* = 7,400 V, *IMAX* = 52 μA), and remaining saturated till (*V* = 2,400 V, *I* = 28 μA).

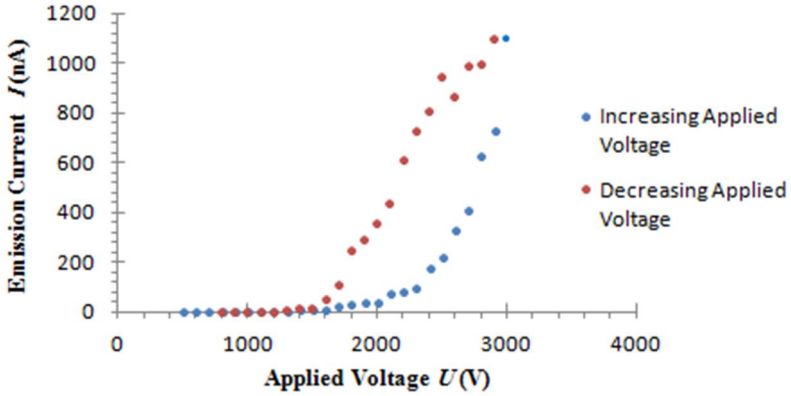

(a)

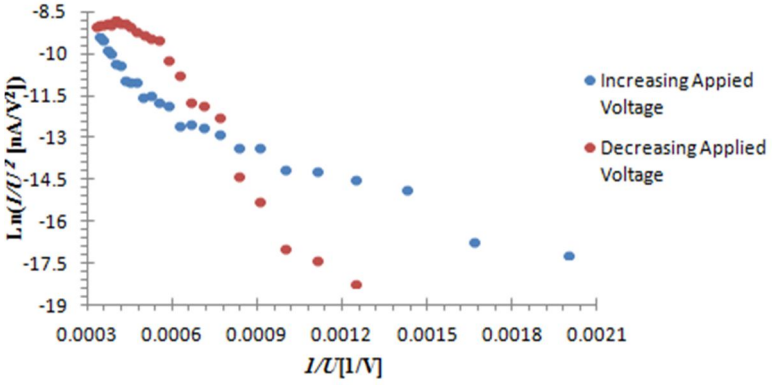

(b)

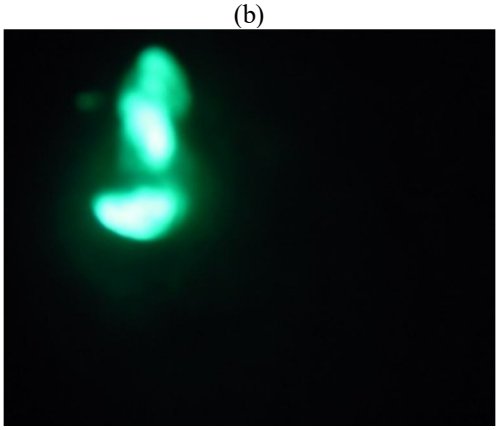

(c)

FIG. 6: First cycle of MWCNT emitter 2 while increasing and decreasing the voltage: (a) *I-V* characteristics, (b) corresponding FN plot for the increasing and decreasing cycle, and (c) emission image with applied voltage reduced to 2,900 V having *I* = 1.1 μA.

In Fig. 7(a), for emitter 2, the applied voltage was increased from V_{TH} = 500 V with I_{TH} = 9.1 pA to the switch-on applied voltage V = 3,000 V with I = 1.1 µA, and then reduced until the applied voltage was V_{TH} = 800 V with I_{TH} = 8.0 pA. The high emission current at a relatively low applied voltage is caused by the sharpness of the emitter (diameter = 183.7 µm). The thickness of the glass and NC7000 MWCNTs powder at the edge of the open end of the glass emitter is shown in Figs. 2(b) and 3(b). These measurements were repeated for a second and third time to see if there was any change in the behavior of the emitter. In the second cycle, there were no changes in the *I-V* characteristics and the emission image. A third cycle, as presented in Fig. 7, was made to obtain more significant current and image stability. The applied voltage was increased from V_{TH} = 800 V with I_{TH} = 8.7 pA to switch-on applied voltage V = 2,700 V with I = 320 nA. Then, the voltage was decreased to V_{TH} = 1,330 V with I_{TH} = 8.2 pA. Fig. 8 shows the results of increasing and decreasing applied voltage.

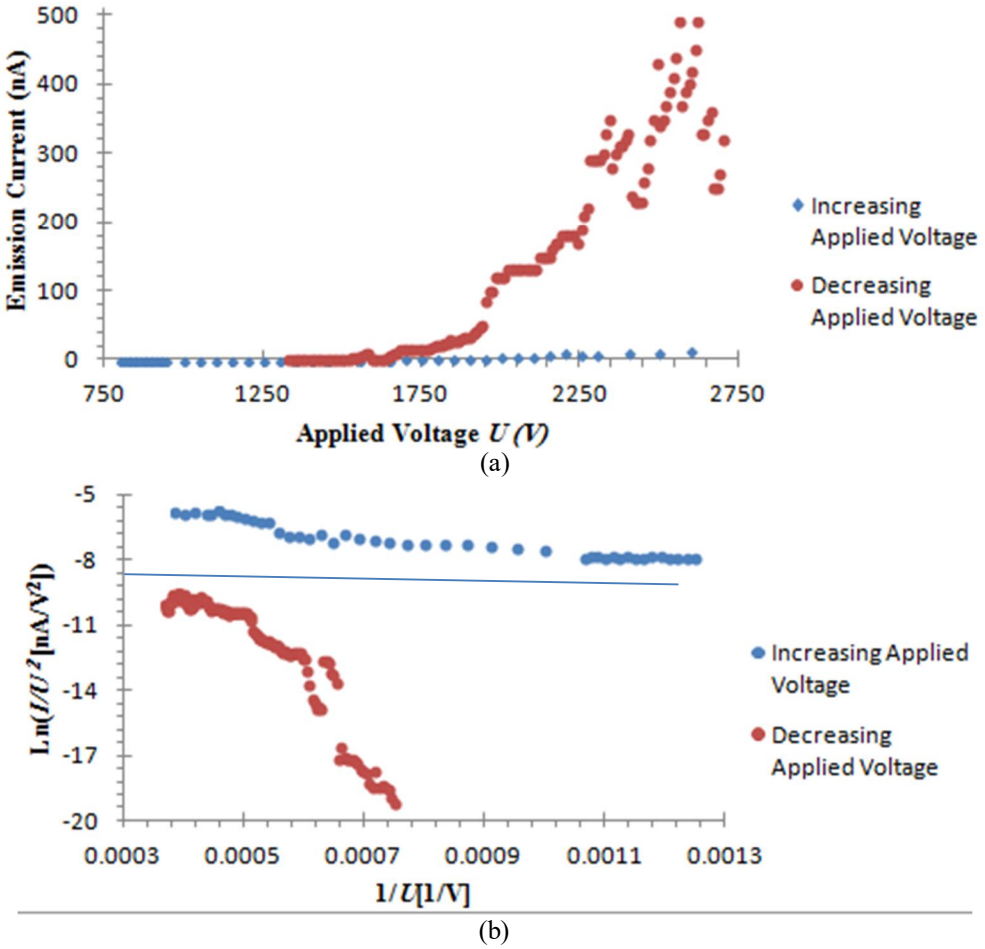

FIG. 7: Third cycle of MWCNT emitter 2: (a) *I-V* characteristics, (b) corresponding FN plot for the increasing and decreasing cycle.

Note that during the first cycle, the initial value of the current is usually higher than its value at the same applied voltage during later cycles due to the initial conditioning of the MWCNTs. Also, in each cycle, as the voltage decreases, the current tends to be higher than when increasing the voltage, indicating hysteresis. This effect may arise because the MWCNTs could be warmer at the same voltage during the descending voltage phase compared to the ascending phase.

Fig. 8 presents the temporary stability of an electron emission image over 40 minutes for a single concentrated spot on a conductive screen. The advantage of using MWCNTs over other emitters arises from their sharpness and intrinsic properties that influence emission performance. Also, it has been reported that MWCNTs have metallic-like characteristics [28, 29], essentially because the I−V characteristics seem to follow the Fowler–Nordheim (FN) linear trend. In contrast, FN plots' deviations, saturation effects,

and discrete current levels are characteristics of materials with non-metallic emitting states, such as nanotips [30, 31]. However, the systematic deviations presented in this study appeared at higher emitted currents. Such deviations are usually connected to the space-charge effects that reduce the FN slope at higher electric fields [32].

Table 1 summarizes the results obtained in this study to make it easier to compare the obtained results.

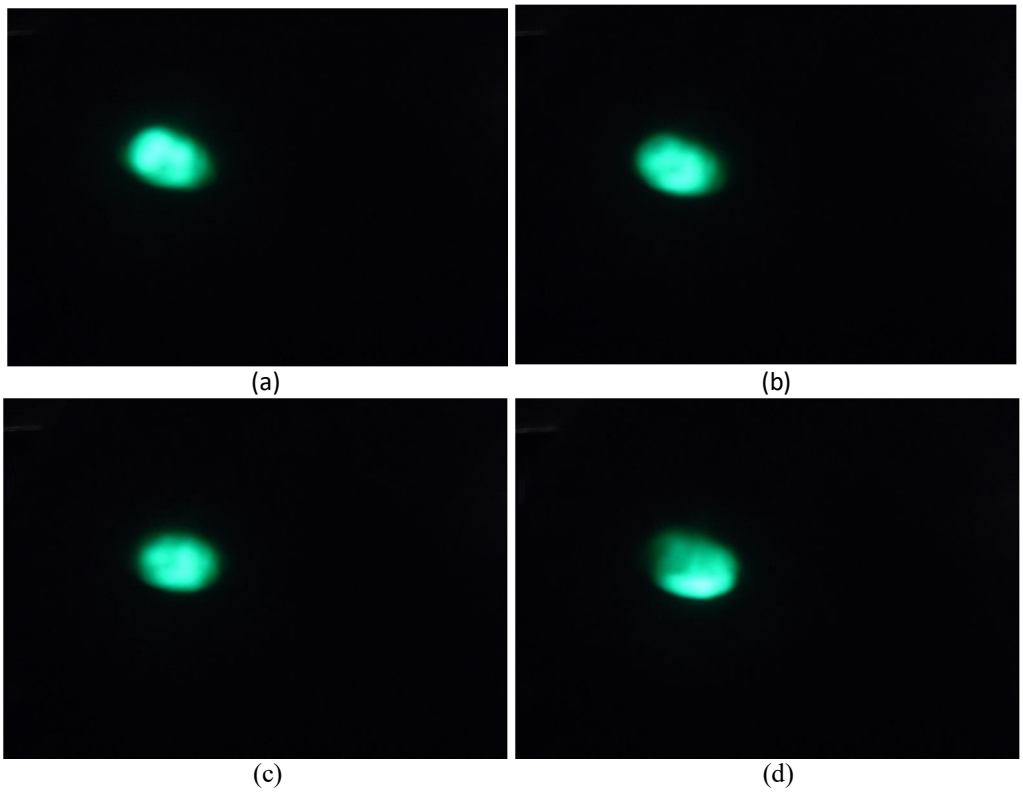

FIG. 8: A sequence of projection images produced showing the temporary stability of the electron emission for MWCNT emitter 2. The sequence of images was recorded at 10-minute intervals with V = 2,350 V and I = 350 n A.

TABLE 1. Summary of the obtained field emission characteristics from multi-walled carbon nanotubes.

Sample	Diameter (μm)	Cycle part	$(I, V)_{threshold}$ (pA, kV)	$(I, V)_{max}$ (μA, kV)	FN-slope (decades.V)
1 (1st cycle)	183.7	Increase	(9.9, 1.5)	(50, 6.1)	–13399.4
		Decrease	(9.7, 1.6)		–10309.5
1 (2nd cycle)		Increase	(9.5, 1.5)	(52, 6.1)	–71428.6
		Decrease	(9.9, 1.7)		–9403.1
2 (1st cycle)	315.0	Increase	(9.1, 0.5)	(1.1, 3)	–3529.41
		Decrease	(8.0, 0.8)		–11931.8
2 (2nd cycle)		Increase	(8.7, 0.8)	(0.32, 2.7)	–30058.6
		Decrease	(8.2, 1.33)		–2000

Changes in the surface geometry, chemical composition, and adsorbate coverage are most likely connected to the current steps [33, 34]. This is unlikely because of the structure of the tube aperture, where any small change in the adsorbate coverage results in significant variations of the work function [34, 35].

Obtaining saturated current with a stable charge distribution on the emitter surface is not fully understood. The solution might be found by presenting a new field emission mechanism, necessitating further research to clarify this aspect. Such emitters might provide an electron source with a stable supply of the emission current for technological applications.

Conclusion

Many electron beam systems, such as electron microscopes, could benefit from the valuable characteristics of a field emission source. For example, the emission characteristics of MWCNTs composite micrometers show several beneficial features, including very high brightness, a high maximum emission current, a reasonably low switch-on voltage, and saturation effects at a higher emission current as shown in Table 1 at the end of the results and discussion section.

Acknowledgment

The authors would like to acknowledge the support of Mu'tah University through the research project \#663/2022.

References

[1] Iijima, S., Nature, 354 (1991) 56.

[2] Alireza, B. and Gordon, M., Chem. Eng. J., 195–196 (2012) 377.

[3] Awasthi, K., Srivastava, A. and Srivastava, O.N., J. Nanosci. Nanotechnol., 5 (10) (2005) 1616.

[4] Ebbesen, T.W. and Ajayan, P.M., Nature, 358 (1992) 220.

[5] Saito, Y. and Uemura, S., Carbon, 38 (2000) 169.

[6] Andrews, R., Jacques, D., Rao, A.M., Rantell, T., Derbyshire, F., Chen, Y., Chen, J. and Haddon, R.C., Appl. Phys. Lett., 75 (1999) 1329.

[7] Tans, S.J., Verschueren, R.M. and Dekker, C., Nature, 393 (1998) 49.

[8] Nakahaea, H., Ichikawa, S., Ochiai, T., Kusano, Y. and Siato, Y., e-J. Surf. Sci. Nanotech., 9 (2011) 400.

[9] El Ghanem, H.M., Jwawad, S.A., Al-Saleh, M.H., Hussain, Y.A. and Salah, W., Elsevier: Phys. B: Condensed Matter, 418 (2013) 41.

[10] Murray, J.J., Lawrence Radiation Laboratory Report (1960).

[11] Latham, R.V., "High Voltage Vacuum Insulation: The Physical Basis". (U.S.A: Academic Press, 1981).

[12] Latham, R.V., IEEE Trans. Insul., 23 (1988) 881.

[13] Bayliss, K.H. and Latham, R.V., Proc. R. Soc. London: A, Mathematical and Physical Sciences, 403 (1986) 285.

[14] Latham, R.V. and Mousa, M.S., J. Phys. D: Appl. Phys., 19 (1986) 699.

[15] Hibbert, R.E. and Robertson, A.J.B., Proc. R. Soc. A, 349 (1976) 63.

[16] Heer, W.A.D., Chatelain, A. and Ugarte, D., Science, 270 (1995) 1179.

[17] Mousa, M.S., Elsevier: Surf. Sci., 246 (1991) 79.

[18] Mousa, M.S. and Hibbert, D.B., Elsevier: Appl. Surf. Sci., 67 (1993) 59.

[19] Mousa, M.S. and Hibbert, D.B., J. Phys. D: Appl. Phys., 26 (1993) 697.

[20] Fowler, R. and Nordheim, L., Proc. R. Soc. Lond. A, 119 (781) (1928) 173.

[21] Gomer, R., Surf. Sci., 299/300 (1994) 129.

[22] Kumar, M. and Ando, Y., J. Nanosci. Nanotechnol., 10 (2010) 3739.

[23] Bani Ali, E.S. and Mousa, M.S., "Switch-on Phenomena and Field Emission", (2016).

[24] Collins, P.G. and Zettl, A., Phys. Rev. B, 55 (1997) 15.

[25] Forbes, R.G., Deane, J.H.B., Fischer A. and Mousa, M.S., Jordan J. Phys., 8 (2015) 125.

[26] Daradkeh, S., Mousa, M.S. and Forbes, R.G., 31st Int. Vac. Nanoelectron. Conf., Kyoto, Japan. (2018).

[27] Al-Qudah, A., Mousa, M.S. and Fischer, A., Mater. Sci. Eng., 92 (2015) 012021.

[28] Bonard, J-M., Maier, F., Stöckli, T., Chatelain, A., de Heer, W.A., Salvetat, J.-P. and Forr'o, L., Ultramicroscopy, 73 (1998) 7.

[29] Wang, Q.H., Corrigan, T.D., Dai, J.Y.R., Chang, P.H. and Krauss, A.R., Appl. Phys. Lett., 70 (1997) 3308.

[30] Thien, V.B., Garcia, N. and Purcell, S.T., Adv. Imaging Electron. Phys., 95 (1996) 63.

[31] Bonard, J-M., Croci, M., Klinke, C., Kurt, R., Noury, O. and Weiss, N., Carbon, 40 (2002) 1715.

[32] Barbour, J.P., Dolan, W.W., Trolan, J.K., Martin, E.E. and Dyke, W.P., Phys. Rev., 92 (1953) 45.

[33] Swanson, L.W. and Bell, A.E., Adv. Electron. Electron Phys., 23 (1973) 193.

[34] Lee, S.C., Irokawa, Y., Inoue, M. and Shimizu, R., Surf. Sci., 330 (1995) 289.

[35] Kyritsakis, A. and Xanthakis, J.P. Proc. R. Soc. A, 471 (2015) 20140811.